NRC Publications Archive
Archives des publications du CNRC

Cellular delivery of plasmid DNA into wheat microspores using rosette nanotubes

Cho, Jae-Young; Bhowmik, Pankaj; Polowick, Patricia L.; Dodard, Sabine G.; El-Bakkari, Mounir; Nowak, Goska; Fenniri, Hicham; Hemraz, Usha D.

National Research Council Canada   Conseil national de recherches Canada

Canada

Article

Cellular Delivery of Plasmid DNA into Wheat Microspores Using Rosette Nanotubes

Jae-Young Cho, Pankaj Bhowmik, Patricia L. Polowick, Sabine G. Dodard, Mounir El-Bakkari, Goska Nowak, Hicham Fenniri,* and Usha D. Hemraz*

Cite This: *ACS Omega* 2020, 5, 24422−24433

Read Online

ACCESS | Metrics & More | Article Recommendations | SI Supporting Information

ABSTRACT: Plant genetic engineering offers promising solutions to the increasing demand for efficient, sustainable, and high-yielding crop production as well as changing environmental conditions. The main challenge for gene delivery in plants is the presence of a cell wall that limits the transportation of genes within the cells. Microspores are plant cells that are, under the right conditions, capable of generating embryos, leading to the formation of haploid plants. Here, we designed cationic and fluorescent rosette nanotubes (RNTs) that penetrate the cell walls of viable

wheat microspores under mild conditions and in the absence of an external force. These nanomaterials can capture plasmid DNA to form RNT−DNA complexes and transport their DNA cargo into live microspores. The nanomaterials and the complexes formed were nontoxic to the microspores.
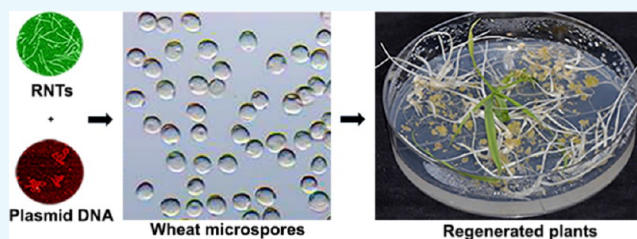
INTRODUCTION

The delivery of nucleic acids into living cells is a highly researched field,[1−3] as it allows the introduction of foreign genes and can suppress disease by replacing defective or undesired genes. Free oligonucleotides have been delivered using various methods such as electroporation, gene guns, and direct injection; however, these are not desirable methods for gene therapy due to rapid DNA or RNA degradation, thermal damage, and subsequent cell death.[4,5] As such, it is important to have a vector that would protect and deliver the cargo to the desired site. Oligonucleotides can be delivered using either a biological (viral or agrobacterium) or a nonviral vector. While viral vectors are highly efficient at delivering nucleic acids, they also have a number of limitations that include toxicity and inflammatory response.[1,2] Nonviral vectors, on the other hand, have low delivery efficiency and gene expression compared to their viral counterparts, but they are usually biocompatible, less toxic and can be synthesized on a large scale.[6] Their applicability in plant systems has been limited not only for their inability to efficiently cross plant cell walls but also due to public acceptance and regulatory limitation in allowing such technologies in the food and crop industries. However, the increasing adoption of genetic engineering and new tools in plant breeding might be the solution to addressing the rising demand for crop production, growing human consumption, changing environmental conditions, and surge in the usage of environmentally friendly and sustainable materials.[7,8]

The plant cell wall has a size exclusion limit of 5−20 nm and nanomaterials[9]—materials possessing at least one dimension measuring 1−100 nm—have driven the pronounced interest in developing nanotechnology-based delivery techniques to transport biomolecules into plant cells.[10] Nanomaterials have been used to bind with biomolecules, protect them from enzymatic degradation,[11] and carry them to a targeted site. For instance, mesoporous silica nanoparticles were successfully used to transport DNA into isolated plant cells, where their cargo was released and expressed.[12] A mechanistic study of cellular uptake using nanoparticles, such as single-walled carbon nanotubes, gold and silica nanoparticles, quantum dots and nanoceria, on plant protoplasts—membrane bound plant cells from which the cell walls have been removed by enzymatic degradation—showed that cellular uptake is dictated by the magnitude of the zeta potential and size of the nanoparticles.[13]

Incubation and topical spraying have been used to deliver nucleic acids and dyes to intact plant cells using clay nanosheets,[14,15] dendrimers, gold nanoparticles, and cell penetrating peptides (CPPs).[16−18] Other methods of delivery include bombardment[19−21] and microinjection[22] using a specialized glass microcapillary injection pipette have been utilized to deliver nanomaterials or nanomaterials-bound molecules and transform a wide range of plant species. These conditions tend to be harsh and result in tissue damage
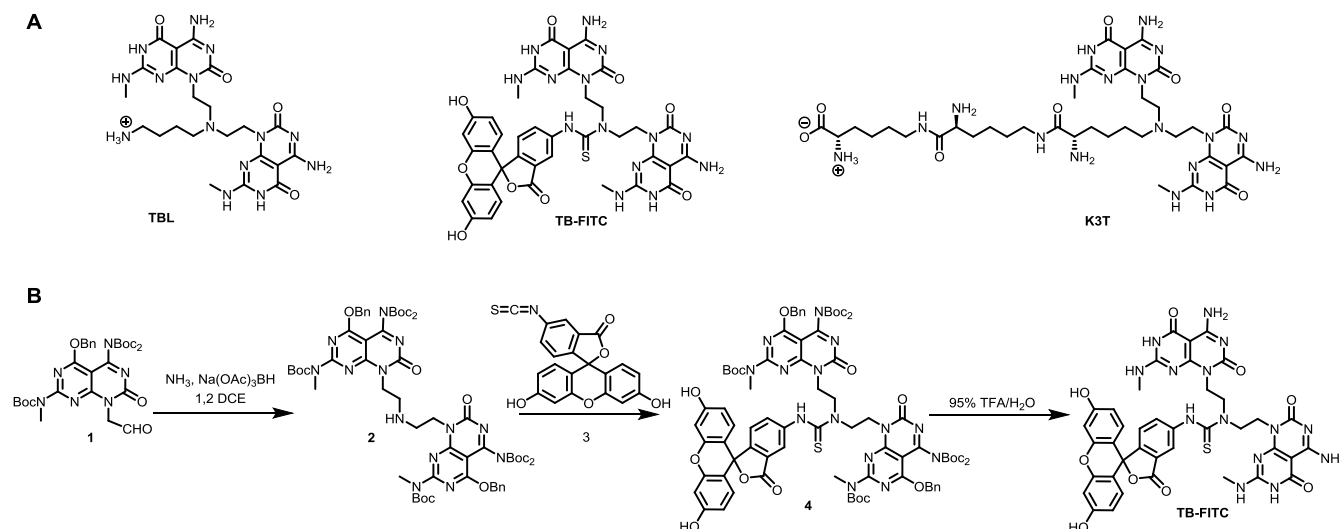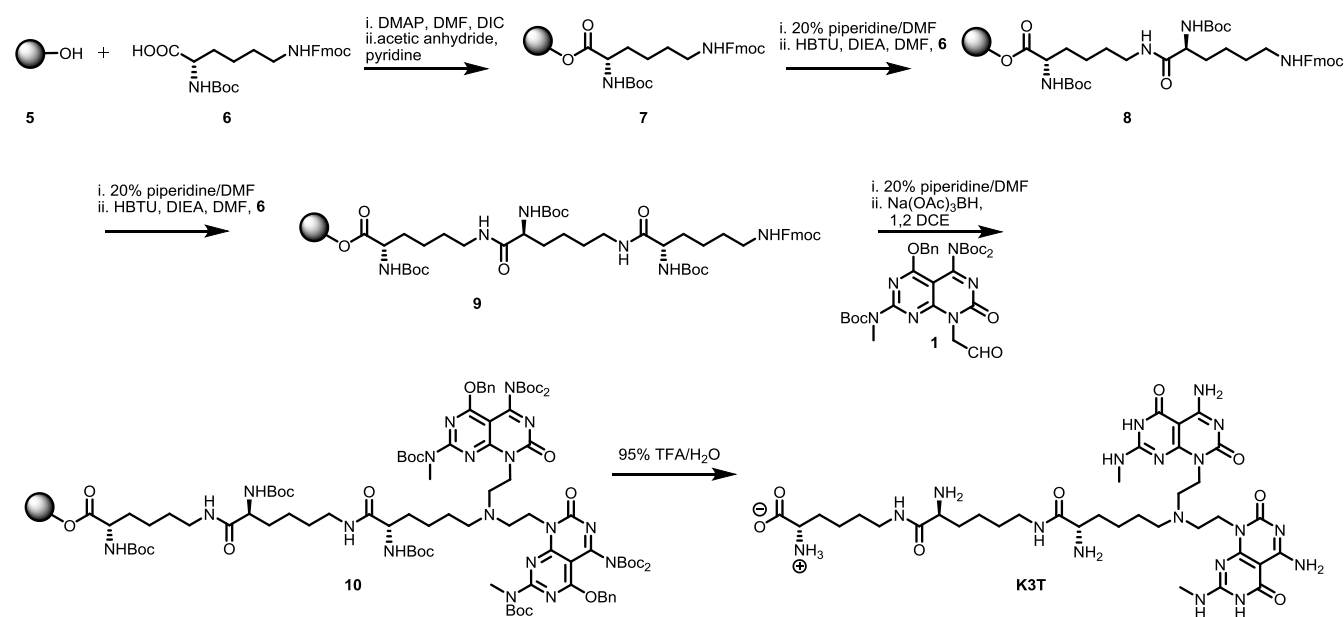
Scheme 1. (A) Structures of TBL (Twin G∧C with an Aminobutane Side Chain), TB-FITC (Twin G^C Functionalized with Fluorescein), and K3T (Twin G∧C Bearing 3 L-Lysine Residues) Motifs and (B) Synthetic Scheme for the Synthesis of TB-FITC

Scheme 2. Synthetic Scheme for the Synthesis of K3T Compound Containing Three Lysine Residues Using SPPS

or are too costly. A faster and cheaper alternative to microinjection is the use of macroinjection, where hypodermic needles are used to inject floral buds. This process allows the transfection of the plant microspores with the genetic materials in vivo and the immature transfected microspores are then isolated and cultured to produce a transgenic doubled haploid plant.[23] Microspores, which are immature pollen grains, have great potential due to their ability to produce mature double haploid plants from single cells under the right treatment conditions, usually involving stress.[24] However, the main hindrance to transfection and reproducibility is the presence of an impervious microspore exine and intine, which limits entry to the cell. The delivery is presumed to occur through the micropore, which is a small opening in the exine. Nevertheless, it has been possible for CPPs to penetrate viable microspores and deliver protein.[24,25] Out of all of these nanomaterials, carbon nanotubes have so far generated the most impact.

Cationic polymers complexed with single-walled carbon nanotubes were successfully used to deliver genetic materials in mature plants through infiltration and into protoplasts.[26,27] This subsequently led to a trail of interesting works. However, the recent addition of carbon nanotubes to the SIN (Substitute It Now) list by ChemSec has likely dampened the scope of carbon nanotubes' applications.[28] While critics argue that grouping all carbon nanotubes and banning them would be unjustified and detrimental to innovation, ChemSec argues that the evaluation is based on hazard identification. As such, there is a need to investigate the use of less toxic materials for applications in the food and crop industries.

Rosette nanotubes (RNTs) are biocompatible nanomaterials that are formed through a self-assembly process of self-complementary guanine−cytosine (G∧C) motifs.[29,30] When in a solution, these compounds self-organize into hexameric supermacrocycles (rosettes), held by 18 or 36 hydrogen

bonds.[29,31−33] These rosettes then $\pi-\pi$ stack to form hollow nanotubes with an internal diameter of 1.1 nm. The size of the outer diameter of the nanotubes depends on the length of the side chain expressed on their surface. The ability to feature various functional groups on their periphery, along with their low toxicity, has led to the design of RNTs for a wide range of biological applications,[34−36] including the support of the growth of a wide range of mammalian cells.[37−46] In this work, nontoxic and biocompatible nanomaterial RNTs were used for delivery into plant cells. Cationic and fluorescent RNTs were complexed with plasmid DNA via noncovalent interactions and delivered into wheat microspores with intact cell wall. Microscopy imaging was conducted throughout to gain a better understanding of the type of interactions, morphologies, aggregation behavior, and size of the complexes formed.

■ RESULTS AND DISCUSSION

Preparation and Characterization of RNTs. The three monomers TBL (a twin G∧C monomer connected by an aminobutane linker), TB-FITC (a twin G∧C monomer functionalized with fluorescein), and K3T (twin G∧C monomer containing three L-lysine residues) (Scheme 1) were synthesized for the preparation of the RNTs used for this study. TBL[33,40] was synthesized according to a previously reported procedure using reductive amination of 1,4-diaminobutane and the G∧C aldehyde **1**.[29] Compound TB-FITC was prepared via a reductive amination of the G∧C aldehyde **1** with ammonia, followed by coupling with fluorescein 5-isothiocyanate and subsequent cleavage of all protecting groups in acidic conditions, as illustrated in Scheme 1. The TB-FITC motif contains a fluorescent moiety, which when coassembled with other self-assembling monomers, would result into heterogeneous fluorescent RNTs that can be tracked.

The K3T[33] is a twin G∧C compound containing three lysine residues; it was prepared using solid-phase synthesis (SPPS) and chemical synthesis (Scheme 2). Standard Fmoc SPPS was first used to prepare the Wang resin-supported tri-lysine peptide **9**, with peptide bonds at the ε-amino group of lysine. The Fmoc protecting group from **9** was removed and the resulting free amino group was coupled with 2 equiv of the G∧C aldehyde **1** by reductive amination using sodium triacetoxyborohydride to produce the protected twin G∧C derivative **10**. Removal of the protecting groups and cleavage from the resin under acidic conditions produced the tri-lysine containing the K3T compound.

Next, the self-assembly of the three motifs TBL, TB-FITC, and K3T were investigated in aqueous solutions. It has been previously shown that monomers containing both single and two G∧C units can produce RNTs through self-assembly.[29,31,32] However, the twin base monomer can form more stable nanotubes as each monomer engages in 12 hydrogen bonds arising from two G∧C units, as opposed to the single G∧C monomer that participates in only six hydrogen bonds. Figure 1 shows how the TBL motifs self-assemble to form RNTs in a solution using molecular models generated through Macromodel 8.5.[32,33] The monomers form six-membered macrocycles (rosettes), held together by 36 H-bonds, compared to 18 H-bonds for rosettes derived from single G∧C monomers. The self-organization of these rosettes through $\pi-\pi$ stacking interactions results in the formation of stable nanotubes. SEM imaging shows how the motifs TBL,
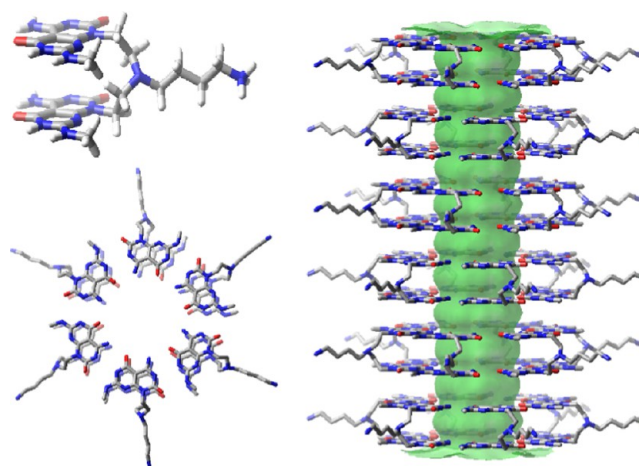

Figure 1. Model showing hierarchical self-assembly of TBL into double-stacked hexamers to produce a hollow nanotube, with an internal diameter of 1.1 nm and an outer diameter of 3.4 nm.

TB-FITC, and K3T produced long and well-dispersed homogeneous RNTs in an aqueous medium (Figure 2).

The efficacy of a nanocarrier depends on its ability to capture and transport its payload into target cells. Cationic polymers have been used as nonviral tools to deliver nucleic acids via the formation of polyplexes. In such cases, it has been reported that their stability relies greatly on chemical composition and molecular weight. However, molecular weight and consequently the size of the nanomaterial formed cannot be used as a sole predictor of how a material will fare in its transfection efficiency. For instance, there have been several conflicting reports of both high- and low-molecular-weight polyethylenimines (PEI), dendrimers, and chitosan having high transfection efficiency.[49−53] In general, polymers with higher molecular weight tend to form stronger and more stable polyplexes with nucleic acids and protect them better. Yet, this property acts as a double-edged sword as the delivery vehicle is unable to release its payload due to the stronger electrostatic interactions.

For the RNTs to act as efficient DNA carriers, they should have the necessary dimensions and charge to penetrate the microspores. Although these RNTs form hollow tubes with an internal diameter of 1.1 nm, it is unlikely that the DNA is captured inside the tubes. Instead, we believe that they form polyplexes through nonspecific binding of the payload to the external surface of the nanotubes. While the RNTs used did have diameters of <5 nm (3.5 ± 0.2 nm for TBL RNTs and 4.4 ± 0.5 nm for K3T RNTs), they could assemble into structures several micrometers in length. Consequently, it was important to devise a way to control the length of the RNTs. Sonication was used to produce short nanotubes, ranging between 100 and 300 nm in length, as seen from the SEM image (Figure 3). In general, aging the RNT samples over time resulted into longer tubes and bundles; however, sonication of samples with different aging time produced comparable shorter tubes. For this study, the TBL and K3T were always used in conjunction with TB-FITC to produce TBL/TB-FITC and K3T/TB-FITC RNTs. Based on earlier reports,[54] our assumption was that TBL (or K3T) and TB-FITC motifs would comix and assemble to produce heterogeneous fluorescent RNTs (Figure 4). An average size of 241 ± 32 nm was observed by DLS for TBL/TB-FITC; this was also in agreement with the SEM and TEM data, which showed short and well-dispersed RNTs.
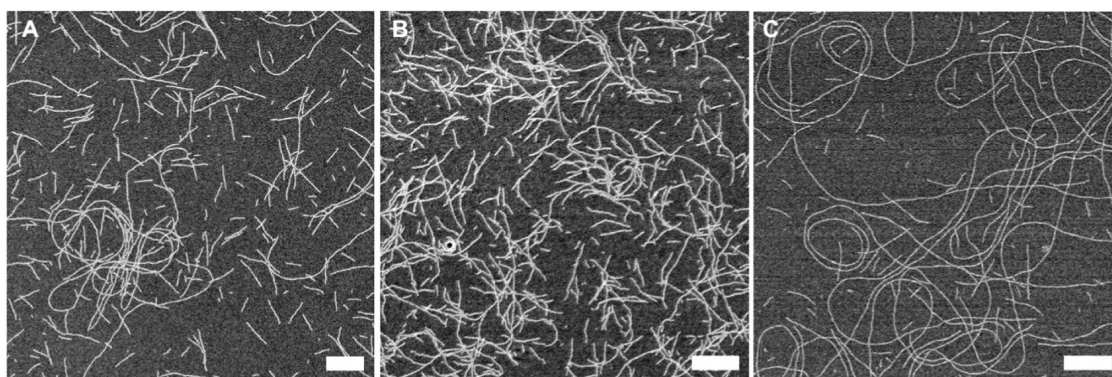
Figure 2. SEM images of TBL (A), K3T RNTs (B), and TB-FITC (C) in water. TBL and K3T RNTs were aged for 1 day, whereas TB-FITC was aged for 7 days. Scale bar = 200 nm.
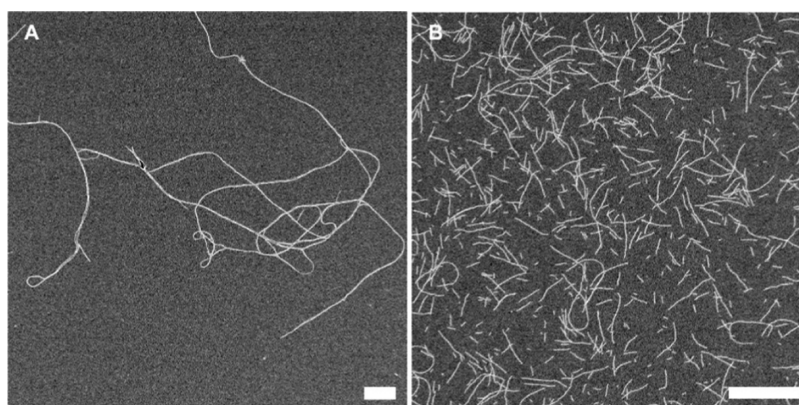

Figure 3. TBL/TB-FITC (A) assembled in water without ultrasonication. Ultrasonication of TBL/TB-FITC RNTs (A) for 15 min produced uniform short nanotubes, ranging 100−300 nm in length, as seen in (B). Scale bar = 500 nm.

Next, the zeta potentials of the materials were measured. The positive charges on polycations are the main reason behind the formation of polyplexes between the positively charged materials and the negatively charged nucleic acid. Yet, this excess of positive charge often leads to cytotoxicity.[55,56] As a result, it was important that the material designed was only mildly positive in the physiological environment. Zeta potential measurements of TBL/TB-FITC showed a value of +27.9 ± 1.8 mV. In general, the zeta potential values for the various nanotubes were about +30 mV.

Characterization of mCherry DNA. The choice of the nucleic acid is crucial in determining the efficiency of a nanocarrier-mediated delivery. The mCherry plasmid DNA was chosen as we had previously investigated it for wheat transformation in wheat embryos using a biolistic gene gun and found that the mCherry reporter was expressing in the bombarded embryos after transformation. The plasmid DNA used did not contain any components that could produce a targeted response in the microspores or the subsequent embryos and plants. Prior to conducting any complexation experiments, the morphology of the various types of mCherry plasmid DNA was investigated using AFM (Figure 5). The circular mCherry plasmid DNA is intact, the linear mCherry plasmid DNA is nicked, and the DNA cassette only contains the elements around the mCherry sequence. Circular mCherry plasmid DNA was subsequently chosen for the complexation and microspore uptake experiments as it had a more distinct morphology, which could be differentiated from the nano-tubes. The zeta potential value of circular mCherry plasmid

DNA was negative (−53.0 ± 1.2 mV), which implied that it could engage in electrostatic interactions with the cationic RNTs to form RNT−DNA complexes.

Complexation of RNTs with Plasmid DNA. Next, the complexation of the RNTs with the circular mCherry plasmid DNA was explored. Gel retardation assay was used to optimize the binding capacity and complex formation of RNTs and mCherry plasmid DNA (Figure 6 and S1 and S2). A 1% (w/v) agarose gel was used to assess complex formation between DNA and the RNTs at different weight ratios with increasing concentration of RNTs. As depicted in Figure 6, the mCherry plasmid DNA shows two bands while the RNT sample does not show any bands on the agarose gel. As the concentration of the RNTs was increased, the intensity of the DNA bands decreased and the formation of the RNTs−DNA complex was observed in the wells. The highest binding capacity of the TBL/TB-FITC and mCherry plasmid DNA was noted at a complexing ratio of 5:1. Beyond this ratio, as the concentration of the RNTs was increased, the DNA bands were no longer visible and the intensity of the RNTs−DNA complex bands in the wells became less intense due to dilution. Similar experiments were conducted on K3T/TB-FITC RNTs, which showed a complexing ratio of about 5:1 with the plasmid DNA. To confirm that the integrity of the DNA was unaffected from the complexation process with the RNTs, release of DNA from the RNT−DNA complex was conducted using dextran sulfate at 0.5 and 4.5 h (Figure S3). In both cases, we observed a release of the DNA, with a higher yield at longer exposure time. A more significant release from TBL/
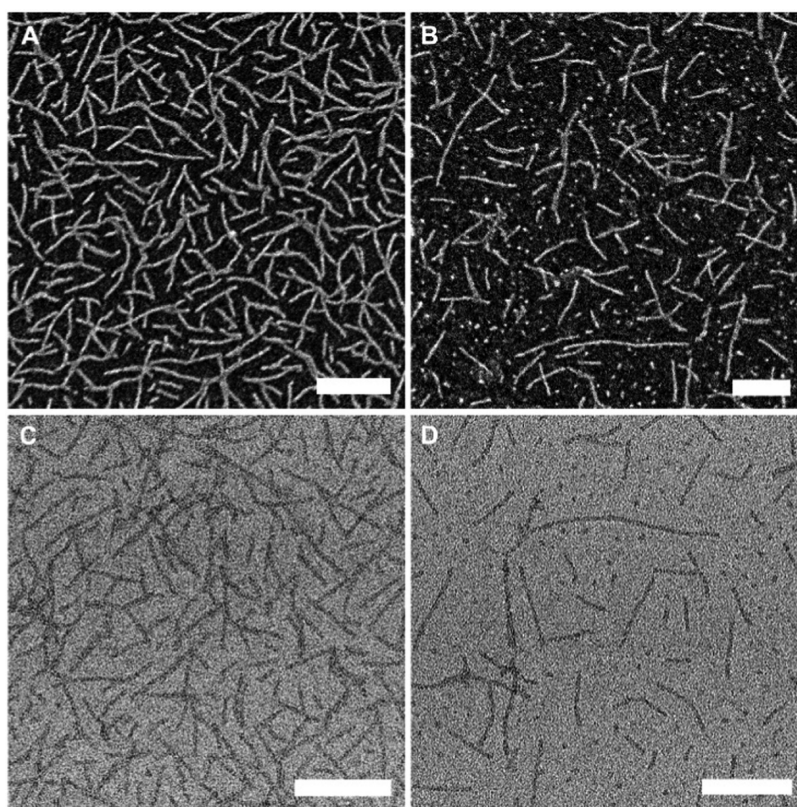
Figure 4. SEM (A, B) and TEM (C, D) images of TBL/TB-FITC (A, C) and K3T/TB-FITC (B, D) (from coassembly and sonication of TBL and TB-FITC, and K3T and TB-FITC). Scale bar = 100 nm.
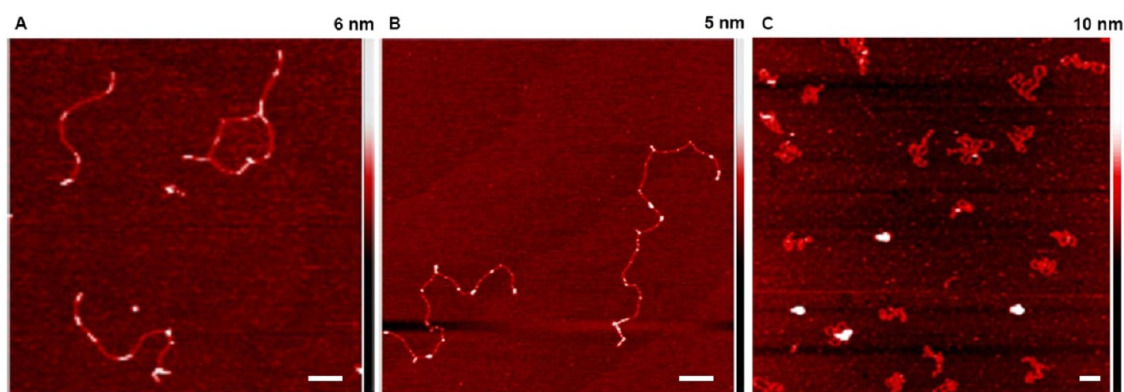
Figure 5. AFM images showing the height profile of plasmid DNA: (A) DNA cassette, (B) linear DNA, and (C) circular mCherry plasmid DNA cast on freshly cleaved mica substrates and imaged under tapping mode. Scale bar = 200 nm.

Well	Sample	Ratio (RNTs/DNA)
1	Ladder	
2	DNA	0
3	TBL/TB-FITC:DNA	0.6
4	TBL/TB-FITC:DNA	1.3
5	TBL/TB-FITC:DNA	2.5
6	TBL/TB-FITC:DNA	5
7	TBL/TB-FITC:DNA	10
8	TBL/TB-FITC:DNA	15
9	TBL/TB-FITC:DNA	20
10	Ladder	

Figure 6. Binding capacity of TBL/TB-FITC: mCherry DNA complexes by gel retardation assay. DNA was mixed with increasing concentration of RNTs and electrophoresed on 1% (w/v) agarose gel.
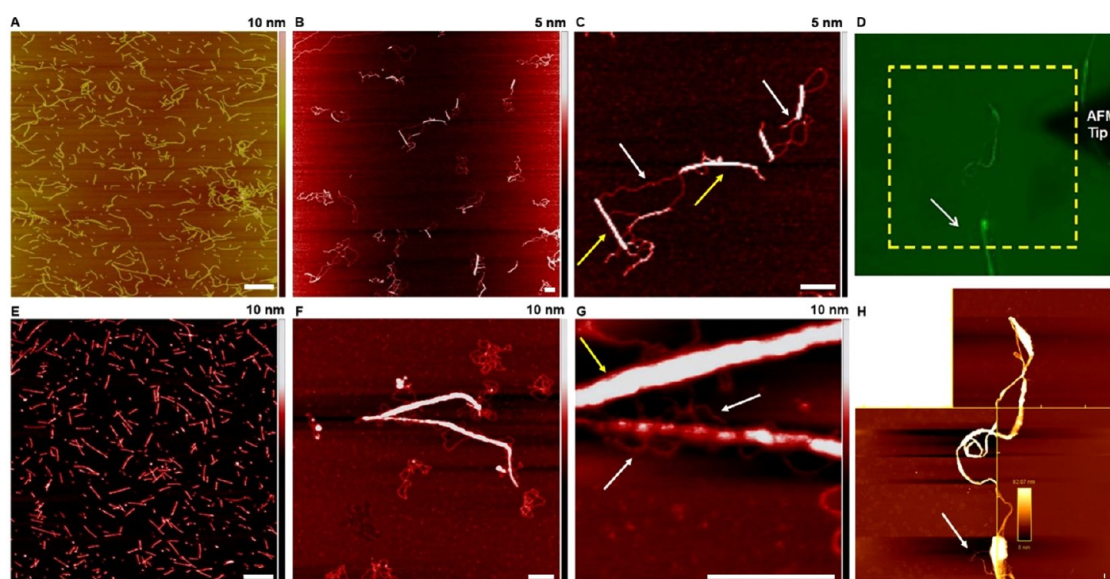
Figure 7. AFM images showing the morphologies from complexation of circular mCherry plasmid DNA with TBL/TB-FITC and K3T/TB-FITC RNTs on freshly cleaved mica substrates: TBL/TB-FITC and K3T/TB-FITC RNTs only (A, E); mCherry DNA with TBL/TB-FITC and K3T/TB-FITC RNTs (B, C, and F, G, respectively); fluorescent microscopic (D) and AFM image of the TBL/TB-FITC−DNA complex (H). The yellow arrows point to the RNTs bundles, while the white arrows correspond to the DNA. Scale bar = 200 nm.

Figure 8. Microscopy images of isolated wheat microspores in a buffer obtained through optical microscopy (A) and SEM images of the microspores cast on a carbon-coated TEM grid (B, C). The image C shows the micropore present on the surface of the microspore through which the cellular uptake is believed to happen. Scale bar = 50 (A), 20 (B), and 2 μm (C).

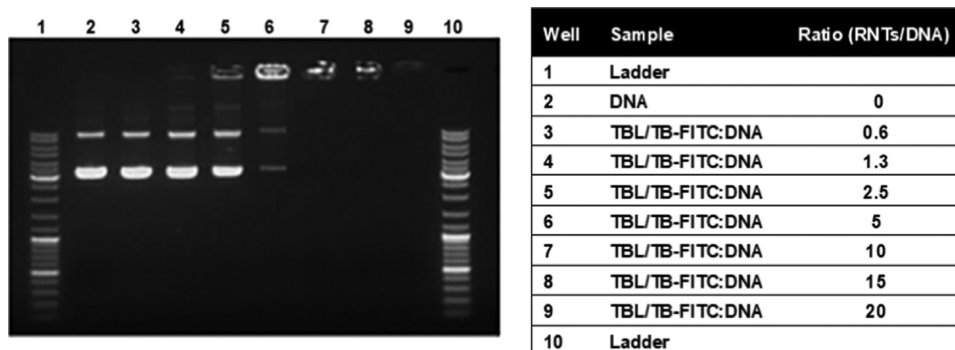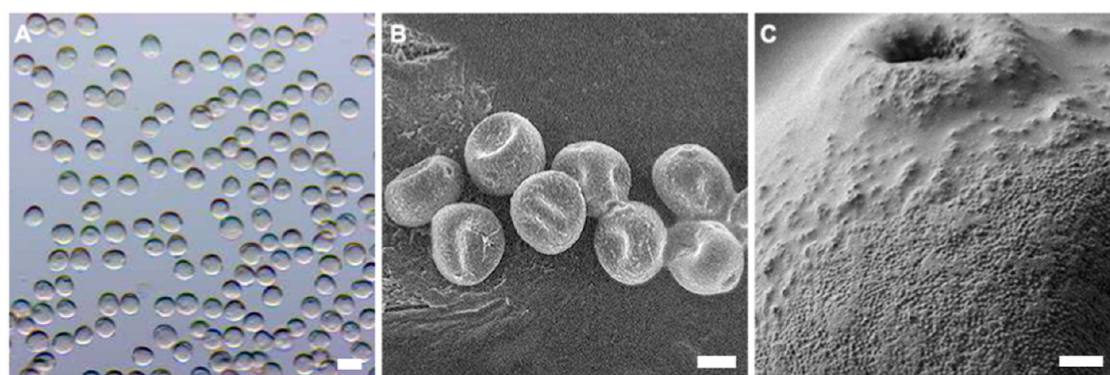TB-FITC than K3T/TB-FITC was observed, which could be due to the stronger electrostatic interactions between the positively charged tri-lysine moiety in K3T and DNA compared to the butyl ammonium on TBL that makes the release of the DNA from the complex more difficult.

The morphology of the RNT−DNA complexes formed was investigated using AFM (Figure 7) and electron microscopy (Figure S4). RNTs and circular mCherry plasmid DNA in a 5:1 ratio (as optimized by gel electrophoresis) were incubated for 0.5 h and deposited on freshly cleaved mica for AFM imaging. As shown in Figure 7, upon complexation, the well-dispersed short tubes (A, E) were replaced by larger aggregates formed due to the attractive electrostatic interactions between the DNA and RNTs, as well as the decrease in the zeta potential values resulting from partial charge neutralization. For the TBL/TB-FITC RNT−DNA complex at a 5:1 ratio, the zeta potential measurements reflected the cationic nature of the complexes formed (+20.1 ± 5.5 mV), which would still facilitate uptake.

It was also possible to see how the DNA strands were wrapped around the RNT bundles (B, C; and F, G). The

average height profile of the RNTs and DNA before and after complexation was measured using AFM and the net increase in the height profile confirmed binding between the RNTs and the plasmid DNA (Figure S5). Furthermore, we used BioScience AFM (D, H), which allows integration of the AFM equipment with other optical methods, to confirm that the DNA and RNTs were complexing. In this case, we were able to visualize the conventional AFM images and the fluorescent images simultaneously. Since the mCherry plasmid DNA used did not have any fluorescent tag, it is not possible to see the DNA in the fluorescent image D; however, it is visibly wrapped around the RNT bundles in the AFM image H, confirming interactions between the nanomaterial and DNA.

With the visual confirmation that the RNTs were successfully complexing with the DNA, we investigated the uptake of both the RNTs and the RNT−DNA complexes by isolated wheat microspores, which are immature pollen grains that can be induced to regenerate into whole plants. The microspores were visualized by SEM (Figure 8) and in-solution AFM (Figure S6). It was also possible to observe the
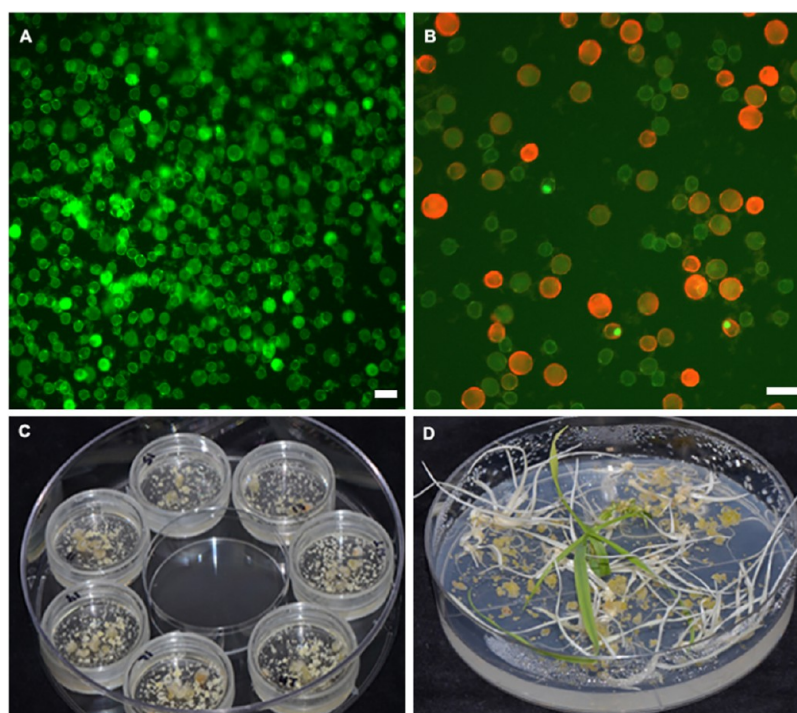
Figure 9. Cellular uptake of TBL-TB-FITC RNTs (A) and TBL-TB-FITC:Cy3-mCherry DNA complexes (B) by wheat microspores, as observed using a Zeiss Axio Xoom V16 fluorescence microscope. The bright green fluorescent color is from the RNTs, while the red fluorescence is from the DNA. Scale bar is 100 μm. Culture of transfected microspores for plant regeneration: embryos (C) and plantlets (D). Scale bar = 200 μm.

micropore on the surface of the microspore, through which the RNTs and complexes penetrate the cells.

The wheat microspores were first incubated with the fluorescent RNT samples for 15 min. After 24 h, it was possible to see an uptake of the TBL/TB-FITC RNTs, as evidenced from the fluorescent microspores obtained using fluorescence microscopy (Figure 9A). These microspores exposed to RNTs were found to remain healthy and divide. The nanomaterials were not found to trigger microspore aggregation or mortality. The uptake of the K3T/TB-FITC RNTs was lower due to the aggregation of the microspores, which could be attributed to the higher positive charges on the tri-lysine chains. With the successful uptake of the RNTs by the microspores, we subsequently evaluated the uptake of the TBL/TB-FITC RNT−DNA complexes, whereby both the RNTs and the DNA were fluorescently labeled. While the RNTs had green fluorescence, the Cy3-labeled DNA showed red fluorescence. It was found to be necessary to label the mCherry plasmid DNA with Cy3, as the DNA alone showed little expression. This was also later found to be the case when using this DNA with other delivery methods. Isolated microspores (100 000 in 100 μL NPB 99 medium) were incubated for 15 min at room temperature with 100 μL of the RNT−DNA complex. After 15 min, the microspores were washed three times with NPB 99 medium to remove all unbound complex. The washed microspores were then plated in 3 mL of fresh NPB medium. Successful uptake of the fluorescence-labeled carrier (green) and plasmid DNA (red) was indirectly confirmed using a Zeiss Axio Xoom V16 fluorescence microscope. After 24 h, it was possible to see that the microspores were successfully transfected with the plasmid DNA. The microspores showed the presence of both red and green fluorescence (Figure 9B), indicative of successful cellular uptake. In addition, there were no unbound RNTs observed in

the solution medium. While it was clear that the FITC-labeled RNTs were internalized and directed into the cell nucleus, it was less clear that the plasmid DNA was still attached, as the Cy3 signal appeared mainly in the cytoplasm. This suggests that the RNTs may function better in a different cell type. The negative surface potential on DNA does not allow DNA alone to enter the microspores, and the RNTs do not only bind with the DNA but also successfully protect and deliver the cargo inside the microspores. After transfection, the microspores were cultured until plant regeneration into embryos (Figure 9C). The FITC-labeled nanomaterial or Cy3-labeled plasmid DNA was observed for up to 72 h as the pooled microspores were allowed to grow. At that point, the signal was diluted either due to growth of the cell or fluorescence degradation. The number and, more importantly, the morphology of those exposed to the RNT−DNA complexes consistently fell within the range of the control. Once the embryos were large enough to evaluate, in the absence of expression of the gene of interest, there was no reason to continue to the plantlet stage. However, the latter was done on a few occasions. Both green shoots and albino shoots, which are an issue in the absence of the RNT−DNA complex, were observed (Figure 9D).

■ CONCLUSIONS

We have demonstrated the ability of RNTs to complex with plasmid DNA and act as a nanocarrier to deliver the cargo into wheat microspores. These nanomaterials, which contained cationic side chains and a fluorescent moiety, were coassembled to generate well-dispersed nanostructures at mildly acidic conditions. The RNTs were found to be nontoxic to the wheat microspores and were internalized by the microspores. The microspores exposed to the complex were found to undergo normal growth for plant regeneration. The fluorescent RNTs were subsequently complexed with plasmid

DNA so that the latter can be protected and transported across the plant cell walls under mild conditions. The resulting nanocomplexes were internalized by the wheat microspores. The transfected microspores were cultured and underwent normal plant regeneration embryo or plantlet stages. The implication of this work is important as it has allowed the delivery of plasmid DNA into wheat microspores using a biocompatible nanocarrier such as the RNTs. While single-walled carbon nanotubes have been used as nanocarriers and were shown to produce a targeted gene expression, the presence and use of carbon nanoparticles in food or agricultural applications is a hotly debated issue due to their potential adverse impact on health.[28,57,58] We are currently working on nanocarrier-mediated delivery that could allow gene silencing or produce a targeted expression.

■ EXPERIMENTAL PROCEDURES

Materials and Methods. Unless stated otherwise, all reactions were performed under N_2 atmosphere. Reagent grade solvents and commercial reagents were purchased from Sigma Aldrich and used without further purification, unless indicated otherwise. Reactions were monitored by TLC using silica-coated TLC plates and were visualized under UV light. The NMR data is presented as follows: chemical shift, multiplicity, coupling constant, and integration. The following abbreviations were used for the multiplicities: s = singlet, d = doublet, t = triplet m = multiplet, and bs = broad singlet. Residual ^1H shifts in CDCl$_3$ (7.24 ppm) and DMSO-d_6 (2.50 ppm), and ^{13}C shifts in CDCl$_3$ (77.23 ppm) and DMSO-d_6 (39.51 ppm) were used as deuterated solvents. The ^1H NMR and ^{13}C NMR spectra were calibrated using 3-(trimethylsilyl)-1-propane-sulfonic acid sodium salt (TMS = 0.0) as the internal reference. The carbon grids used for microscopy were purchased from Electron Microscopy Sciences. Agarose gels, used for gel electrophoresis, were prepared using ultrapure agarose and stained using SYBR safe, both of which were purchased from Life Technologies. The loading dye GelPilot 239901 and GeneRuler SM0333 were purchased from Quiagen and Thermofisher Scientific, respectively. The 1× TAE buffer was prepared from dilution of concentrated 50× TAE from Biorad and was run for 1 h at 100 V for each gel in the electrophoresis system Mini Sub cell GT (BioRad). DNase- and RNase-free water was used throughout the experiment. Plasmid DNA, which expressed the red fluorescent protein mCherry, was either produced in our laboratory or in bulk through GENEWIZ. The original mcherry plasmid vector (Figure S7) came from François Eudes' laboratory (AAFC, Lethbridge, AB, Canada) under our initial evaluation CPPs. DNA samples produced by GENEWIZ were subjected to an extra wash to reduce the amount of salt. The plasmid DNA was labeled using LabelIT Cy3 dye from Mirus, using the labeling procedure available from their website.

Chemical Synthesis. *Synthesis of Compound 2 (Scheme 1).* Compound 1[29] (0.400 g, 0.625 mmol) was added to a solution of 7 M NH$_3$ in MeOH (0.100 mL, 0.700 mmol) in 1,2-dichloroethane (1,2-DCE, 30 mL) at room temperature under N_2 and sonicated for 10 s. The reaction mixture was stirred for 2 h, after which sodium triacetoxyborohydride (0.078 g, 0.372 mmol) was added and the resulting mixture was stirred for an additional 5 h. Another aliquot of sodium triacetoxyborohydride (0.078 g, 0.372 mmol) was added to the reaction mixture and stirred for an additional 15 h. The reaction mixture was diluted with CH$_2$Cl$_2$ (50 mL) and

washed with water (10 mL), brine (15 mL), dried over Na$_2$SO$_4$, and concentrated. Flash chromatography of the residue over silica gel (0−5% MeOH in CH$_2$Cl$_2$) gave **2** (0.326 g, 83%) as a white foam. R_f = 0.56 (5% MeOH in CH$_2$Cl$_2$); ^1H NMR (500 MHz, CDCl$_3$) δ (ppm): 7.47−7.31 (m, 10H), 5.58 (s, 4H), 4.37 (t, J = 7.0 Hz, 4H), 3.50 (s, 6H), 2.90 (t, J = 6.9 Hz, 4H), 1.75 (bs, 1H), 1.56 (s, 18H), and 1.30 (s, 36H); ^{13}C NMR (125 MHz, CDCl$_3$) δ (ppm): 165.6, 161.1, 161.0, 160.3, 155.8, 152.5, 149.2, 134.9, 128.6, 128.5, 128.4, 92.9, 83.6, 83.0, 70.0, 46.7, 43.1, 34.9, 28.1, and 27.8; HRMS: calcd for C$_{62}$H$_{84}$N$_{13}$O$_{16}$N [M + H]$^+$: 1266.6154; found: 1266.6159.

Synthesis of Compound 4 (Scheme 1). Fluorescein 5-isothiocyanate **3** (0.089 g, 0.229 mmol) and N,N′-diisopropyl-amine (0.082 mL, 0.473 mmol) were added to a solution of compound **2** (0.298 g, 0.235 mmol) in ethanol (10 mL) and stirred for 36 h in the dark. The solvent was removed under reduced pressure and the residual oil was dissolved in ethyl acetate, washed with HCl (0.5 M, 10 mL), water (10 mL), brine (15 mL), dried over Na$_2$SO$_4$, and concentrated. Flash chromatography of the residue over silica gel (0−5% MeOH in CH$_2$Cl$_2$) gave **4** (0.280 g, 72%) as a yellow foam. R_f = 0.29 (5% MeOH in CH$_2$Cl$_2$); ^1H NMR (600 MHz, CDCl$_3$) δ (ppm): 9.76 (s, 1H), 8.29 (s, 1H), 7.77 (bs, 1H), 7.45−7.32 (m, 12H), 6.93 (m, 1H), 6.66 (s, 2H), 6.57 (d, J = 7.8 Hz, 2H), 6.39 (d, J = 7.8 Hz, 2H), 5.58 (s, 4H), 4.88−4.40 (m, 5H), 4.38−3.78 (m, 5H), 3.57 (s, 6H), 1.75 (bs, 1H), 1.56 (s, 18H), and 1.31 (s, 36H); ^{13}C NMR (150 MHz, CDCl$_3$) δ (ppm): 181.9, 169.2, 165.8, 161.5, 161.1, 160.9, 158.8, 156.5, 152.6, 152.4, 149.6, 141.8, 134.8, 132.7, 129.3, 128.6, 128.6, 128.5, 127.5, 123.8, 121.6, 112.3, 110.8, 102.9, 93.3, 84.6, 70.4, 40.3, 35.4, 29.7, 28.0, and 27.8; HRMS: calcd for C$_{83}$H$_{93}$N$_{14}$O$_{21}$S [M − H]$^-$: 1653.6360; found: 1653.6366.

Synthesis of Compound TB-FITC (Scheme 1). Compound **4** (0.150 g, 0.091 mmol) was stirred in 95% TFA in water (10 mL) for 2.5 h. Et$_2$O (50 mL) was then added to the reaction mixture to give a white precipitate, which was centrifuged down. The residual solid was resuspended in Et$_2$O, sonicated, and centrifuged down. This process was repeated until the spotting of the Et$_2$O produced no UV active spot. The yellow solid was dried to yield compound **5** (0.086 g, 67%) as an orange powder. ^1H NMR (600 MHz, DMSO-d_6) δ (ppm): 12.22 (s, 2H), 10.41 (bs, 2H), 9.42 (s, 1H), 9.14−8.64 (m, 5H), 8.07 (bs, 2H), 7.80 (s, 1H), 7.58 (d, J = 7.8 Hz, 1H), 7.09 (d, J = 7.8 Hz, 1H), 6.66 (d, J = 1.8 Hz, 2H), 6.60−6.51 (m, 4H), 4.36 (bs, 4H), 4.14 (bs, 4H), and 2.92 (d, J = 4.8 Hz, 3H); ^{13}C NMR (150 MHz, DMSO-d_6) δ (ppm): 182.4, 168.8, 161.8, 160.5, 159.9, 156.6, 155.9, 152.3, 148.9, 148.0, 142.8, 131.3, 129.4, 126.5, 123.7, 118.9, 113.2, 110.1, 102.7, 82.6, 46.0, 40.5, 39.0, and 28.5; HRMS: calcd for C$_{39}$H$_{33}$N$_{14}$O$_9$S [M − H]$^-$: 873.2276; found: 873.2271; elemental analysis: calcd (%) for (C$_{39}$H$_{34}$N$_{14}$O$_9$S)(TFA)$_{2.9}$(H$_2$O)$_3$, MW = 1259.56: C, 42.72; H, 3.43; N, 15.57; S, 2.55; found C, 42.69; H, 3.49; N, 15.86; S, 2.35.

Synthesis of Compound K3T (Scheme 2). Standard Fmoc solid-phase peptide synthesis was used to prepare the Wang resin-supported K$_3$ peptide. The anchoring of the first lysine residue to the resin was carried out in a disposable plastic syringe by reacting the Wang resin (1 equiv) with Boc-Lys(Fmoc)-OH (4 equiv) in the presence of p-dimethylami-nopyridine (DMAP) (1 equiv) in N,N-dimethylformamide (DMF, 8 mL). After activating the resin for 20 min, N,N′-diisopropylcarbodiimide (DIC, 4 equiv) was added to the

vessel and the reaction mixture was shaken for 6 h. The resin was then filtered under vacuum, washed with 10 mL each of CH_2Cl_2, MeOH, DMF, and then treated with 50:50 acetic anhydride/pyridine (5 mL, 1×10 min and 2×20 min) to cap the unreactive hydroxyl groups. The resin was then filtered and washed with $(3 \times 10$ mL) DMF, CH_2Cl_2, and MeOH and dried under vacuum. The substitution degree (0.46 mmol/g) was determined by spectroscopic quantification of the fulvene-piperidine adduct at 301 nm on a resin sample. The subsequent lysine residues were coupled as follows: the Fmoc protecting group was removed by incubation of the resin in 20% piperidine/DMF (5 mL, 1×5 min, 1×30 min). The resulting peptidyl resin was washed with 10 mL each of CH_2Cl_2, MeOH, and DMF. *N*-Ethyl-*N*-isopropylpropan-2-amine (DIEA, 8 equiv) was added to Boc-Lys(Fmoc)-OH (4 equiv relative to resin loading) and 2-(1*H*-benzotriazol-1-yl)-1,1,3,3-tetramethyluronium hexafluorophosphate (HBTU, 4 equiv) in the DMF solution, and the mixture was activated by shaking for 3 min. The resulting mixture was then added to the peptidyl resin and was shaken for 3 h. The peptidyl resin was then drained and washed with 10 mL each of CH_2Cl_2, MeOH, and DMF. The absence of free amino groups was confirmed by a yellow color in the Kaiser test, while the presence of free amino groups is indicated by a blue color. The Fmoc protecting group was removed by incubation of the resin in 20% piperidine/DMF (5 mL, 1×5 and 1×30 min). The resulting peptidyl resin was washed with 10 mL each of CH_2Cl_2, MeOH, and DMF. The Wang resin-supported K_3 tripeptide was coupled to the G∧C aldehyde **1**. The latter (4 equiv relative to resin loading) was added to the peptidyl resin in 1,2-DCE (5 mL), and the mixture was shaken for 4 h. $NaBH(OAc)_3$ (2 equiv) and DIEA (4 equiv) were then added and the mixture was shaken for 36 h, after which another 2 equiv $NaBH(OAc)_3$ and 4 equiv of DIEA were added and shaken for an additional 36 h. The resin was drained and the resulting peptidyl resin was washed with CH_2Cl_2, MeOH, and DMF (4×10 mL each) and dried under vacuum. Cleavage from the resin and deprotection was achieved by treating the resin with 95% TFA/water for 2 h. The beads were filtered over celite, and the resulting filtrate was concentrated to a viscous liquid (rotavap). Cold Et_2O was then added to precipitate the crude K3T compound, which was isolated by centrifugation. The supernatant liquid was removed by decantation. The residual solid was resuspended in Et_2O (2 $\times$ 15 mL), sonicated, and centrifuged. The precipitate was dried to produce the desired K3T as an off-white powder in a quantitative yield. ^{1}H NMR (600 MHz, H_2O/D_2O 90%) δ (ppm): 9.16 (bs, 4H), 8.20−8.14 (m, 9H), 7.70−7.69 (m, 2H), 4.45−4.35 (m, 4H), 3.90 (t, *J* = 6.6 Hz, 1H), 3.81−3.77 (m, 2H), 3.54 (m, 4H), 3.35−3.33 (m, 2H), 3.12−3.04 (m, 4H), 2.85 (s, 6H), 1.85−1.67 (m, 8H), and 1.44−1.21 (m, 10H); ^{13}C NMR (150 MHz, H_2O/D_2O 90%) δ (ppm): 172.8, 170.3, 170.0, 163.1, 160.8, 156.9, 156.5, 150.1, 83.5, 54.4−53.7, 53.5, 51.0, 40.0, 37.5, 31.4, 31.2, 30.3, 28.5, 28.6, and 23.1−22.2; Positive ESI-MS: Calcd for $C_{36}H_{58}N_{18}O_8$ 870.5; found 436.2 $[M + 2H]^{2+}$ (100%), 291.2 $[M + 3H]^{3+}$ (29%); HRMS: calcd for $C_{36}H_{60}N_{18}O_8$ $[M + 2H]^+$: 872.4830; found: 436.2415; Elemental analysis: Calculated for $C_{36}H_{58}N_{18}O_8(CF_3CO_2H)_{4.5}(H_2O)_2(C_4H_{10}O)$, MW = 1493.53: C 39.39, H 5.16, and N 16.87; found: C 39.51, H 5.21, and N 16.53.

Self-Assembly to Produce RNTs. A stock solution of TBL/TB-FITC was prepared in 0.05 M HEPES buffer (pH 5)

at a concentration of 0.5 mg/mL at a ratio of 9:1 using 0.4 mg of TBL for every 0.1 mg of TB-FITC per mL of buffer. The suspension was sonicated and heated to 70 °C for about 3 min to increase the solubility of TB-FITC. The sample was allowed to stand at room temperature in the dark after which decantation was used to separate the solution from any undesired insoluble particles. The stock solution was aged for at least 1 day at room temperature in the dark prior to its use. For subsequent use, the stock solution was kept in the dark at 4 °C. K3T/TB-FITC was prepared in a similar fashion at a concentration of 1.0 mg/mL at a ratio of 9:1 using 0.9 mg of K3T for every 0.1 mg of TB-FITC per mL of buffer. For all experiments, diluted RNT solutions were prepared by dilution of aliquots of the stock solutions with deionized water.

Dynamic Light Scattering (DLS) and Zeta Potential Measurements. DLS and zeta potential measurements were carried out using a Malvern Zetasizer Nano-S instrument. This instrument is equipped with a 4.0 mW He−Ne laser (l = 633 nm) and an Avalanche photodiode detector and works at a 173° scattering angle. DLS was used to determine the relative sizes of the structures formed and does not reflect the actual sizes of the structures since the RNTs, DNA, and complexes are nonspherical. However, the relative sizes obtained give a good indication of the scale of the materials. For the experiments, the materials were dispersed in deionized water. Prior to the measurements, the suspensions (0.1 wt %) were equilibrated at room temperature for 10 min in a temperature-regulated cell at 25.0 ± 0.1 °C. Triplicates were measured for each sample, and averages are reported.

Complexation of RNTs with Plasmid DNA. Unless stated otherwise, for all experiments, aliquots of the stock RNTs solution were diluted with deionized water (50 μL of stock solution to 1950 μL of deionized water) and sonicated for 15 min at RT using a standard ultrasonication bath prior to use to avoid possible aggregation. The resulting solution (100 μL) was then mixed with 2 μL of plasmid DNA (1 μg/μL) and 98 μL of nuclease-free water, and the resulting solution (200 μL) was incubated for 30 min prior to sample preparation for microscopy.

Microscopy. Electron microscopy (scanning electron microscopy (SEM), transmission electron microscopy (TEM), and atomic force microscopy (AFM)) was used to characterize the morphology, aggregation behavior, and size of the nanomaterials, plasmid DNA, and RNT−DNA complexes. The microscopy procedures are described in the Supporting Information.

Determination of Complexing Ratio Using Agarose Gel Electrophoresis. The complexation and decomplexation of plasmid DNA with nanocarriers (K3T and TBL RNTs) were evaluated using agarose gel electrophoresis. The DNA was visualized in the gel by the addition of SYBR safe, which binds strongly to DNA by intercalating between the bases. The dye is fluorescent and it absorbs invisible UV light and transmits the energy as visible orange light. The quality and concentration of the DNA were confirmed using a Nanodrop 1000 (Thermofisher Scientific). The DNA sample was diluted with DNase and RNase-free water before quantification, and the quality of DNA was evaluated using the absorbance 260/280 ratio, which was 1.8 or higher. The nanocarrier was prepared in water at various concentrations and mixed with plasmid DNA to yield different mass ratios. For comparative purposes, the concentration of DNA was kept constant. The resulting samples were then mixed with loading dye and loaded

on an agarose gel and run for 1 h at 100 V in the electrophoresis system.

Plant Material and Microspore Extraction. Seeds of the spring wheat cultivar AC Nanda were obtained from Agriculture and Agri-Food Canada. These were grown and used as donor plants of microspore. The wheat microspores were isolated as previously described by Bhowmik et al.,[47] as adapted from Eudes and Amundsen.[48] Prior to microspore extraction, tillers were harvested from plants before the spike emerged from the boot and kept in the dark at 4 °C for 21 ± 3 days in distilled water. The late uninucleate stage of microspores was verified using a median floret and acetocarmine staining. The spikes were removed from the boot, sterilized, and anthers were excised and placed into the extraction buffer. Anthers were macerated using a 110 mL Warring blender cup (VWR international, #58983-093) strained through a 70 μm filter (VWR International, #CA21008-950) and washed several times with the extraction buffer by centrifugation using a swinging bucket rotor. Finally, cells were resuspended in NPB99 liquid media[49] and used for the incubation and uptake experiments.

Cellular Uptake by Wheat Microspores (Immature Pollen). Cellular uptake of the nanomaterials and the DNA-nanomaterial complexes was evaluated using fluorescence microscopy. Isolated wheat microspores (100 000 in 100 μL NPB 99 medium) were incubated for 15 min at room temperature with 100 μL of the complex/or nanomaterial solution. After 15 min, the microspores were washed three times with NPB 99 medium to remove all unbound materials. Washed microspores were then plated in 3 mL of fresh NPB medium. Successful uptake of the fluorescence-labeled carrier (green) and plasmid DNA (red) was indirectly confirmed using a Zeiss Axio Xoom V16 fluorescence microscope. Only microspores showing both green and red fluorescence were considered as successful cellular uptake event for uptake involving the DNA-nanomaterial complexes.

ASSOCIATED CONTENT

Supporting Information

The Supporting Information is available free of charge at https://pubs.acs.org/doi/10.1021/acsomega.0c02830.

> It contains microscopy procedures, gel electrophoresis, microscopy data, vector map of mCherry plasmid DNA, and background fluorescence for a nontransformed control for wheat microspore (PDF)

AUTHOR INFORMATION

Corresponding Authors

Hicham Fenniri − *Nanotechnology Research Centre, National Research Council of Canada, Edmonton, Alberta T6G 2M9, Canada; Departments of Chemical, Biomedical Engineering, Chemistry and Chemical Biology, Northeastern University, Boston, Massachusetts 02115, United States;* orcid.org/0000-0001-7629-7080; Email: h.fenniri@northeastern.edu

Usha D. Hemraz − *Aquatic and Crop Resource Development, National Research Council of Canada, Montreal, Quebec H4P 2R2, Canada; Nanotechnology Research Centre, National Research Council of Canada, Edmonton, Alberta T6G 2M9, Canada;* orcid.org/0000-0001-5151-9484; Email: Usha.Hemraz@nrc-cnrc.gc.ca

Authors

Jae-Young Cho − *Nanotechnology Research Centre, National Research Council of Canada, Edmonton, Alberta T6G 2M9, Canada*

Pankaj Bhowmik − *Aquatic and Crop Resource Development, National Research Council of Canada, Saskatoon, Saskatchewan S7N 0W9, Canada*

Patricia L. Polowick − *Aquatic and Crop Resource Development, National Research Council of Canada, Saskatoon, Saskatchewan S7N 0W9, Canada*

Sabine G. Dodard − *Aquatic and Crop Resource Development, National Research Council of Canada, Montreal, Quebec H4P 2R2, Canada*

Mounir El-Bakkari − *Nanotechnology Research Centre, National Research Council of Canada, Edmonton, Alberta T6G 2M9, Canada*

Goska Nowak − *Aquatic and Crop Resource Development, National Research Council of Canada, Saskatoon, Saskatchewan S7N 0W9, Canada*

Complete contact information is available at:
https://pubs.acs.org/10.1021/acsomega.0c02830

Notes

The authors declare no competing financial interest.

ACKNOWLEDGMENTS

REFERENCES

(1) Verma, I. M.; Somia, N. Gene Therapy - Promises, Problems and Prospects. *Nature* **1997**, *389*, 239−242.

(2) Crystal, R. G. Transfer of Genes to Humans: Early Lessons and Obstacles to Success. *Science* **1995**, *270*, 404−410.

(3) Kay, M. A.; Rothenberg, S.; Landen, C. N.; Bellinger, D. A.; Leland, F.; Toman, C.; Finegold, M.; Thompson, A. R.; Read, M. S.; Brinkhous, K. M.; et al. In Vivo Gene Therapy of Hemophilia B: Sustained Partial Correction in Factor IX-Deficient Dogs. *Science* **1993**, *262*, 117−119.

(4) Plews, J. R.; Li, J. L.; Jones, M.; Moore, H. D.; Andrews, P. W.; Na, J.; et al. Activation of Pluripotency Genes in Human Fibroblast Cells by a Novel mRNA Based Approach. *PLoS One* **2010**, *5*, No. e14397.

(5) Long, J.; Kim, H.; Kim, D.; Lee, J. B.; Kim, D.-H. J. A Biomaterial Approach to Cell Reprogramming and Differentiation. *J. Mater. Chem. B* **2017**, *5*, 2375−2389.

(6) Mintzer, M.; Simanek, E. E. Nonviral Vectors for Gene Delivery. *Chem. Rev.* **2009**, *109*, 259−302.

(7) Ray, D. K.; Mueller, N. D.; West, P. C.; Foley, J. A. Yield Trends are Insufficient to Double Global Crop Production by 2050. *PLoS One* **2013**, *8*, No. e66428.

(8) Zhao, C.; Liu, B.; Piao, S.; Wang, X.; Lobell, D. B.; Huang, Y.; Huang, M.; Yao, Y.; Bassu, S.; Ciais, P.; et al. Temperature Increase Reduces Global Yields of Major Crops in Four Independent Estimates. *Proc. Natl. Acad. Sci. USA* **2017**, *114*, 9326−9331.

(9) Wang, P.; Lombi, E.; Zhao, F.-J.; Kopittke, P. Nanotechnology: a new opportunity in plant sciences. *Trends Plant Sci.* **2016**, *21*, 699−712.

(10) He, X. X.; Wang, K. M.; Tan, W. H.; Liu, B.; Lin, X.; He, C. M.; Li, D.; Huang, S. S.; Li, J. Bioconjugated Nanoparticles for DNA Protection from Cleavage. *J. Am. Chem. Soc.* **2003**, *125*, 7168−7169.

(11) Torney, F.; Trewyn, B. G.; Lin, V. S. Y.; Wang, K. Mesoporous Silica Nanoparticles Deliver DNA and Chemicals into Plants. *Nat. Nanotechnol.* **2007**, *2*, 295−300.

(12) Lew, T. T. S.; Wong, M. H.; Kwak, S.-Y.; Sinclair, R.; Koman, V. B.; Strano, M. S. Rational Design Principles for the Transport and Subcellular Distribution of Nanomaterials into Plant Protoplasts. *Small* **2018**, *14*, No. 1802086.

(13) Bao, W.; Wang, J.; Wang, Q.; O'Hare, D.; Wan, Y. Layered Double Hydroxide Nano-transporter for Molecule Delivery to Intact Plant Cells. *Sci. Rep.* **2016**, *6*, No. 26738.

(14) Mitter, N.; Worrall, E. A.; Robinson, K. E.; Li, P.; Jain, R. G.; Taochy, C.; Fletcher, S. J.; Carroll, B. J.; Lu, G. Q. M.; Xu, Z. P. Clay Nanosheets for Topical Delivery of RNAi for Sustained Protection against Plant Viruses. *Nat. Plants* **2017**, *3*, 16207.

(15) Samuel, J. P.; Burroughs, F.; Zettler, M. W.; Dixit, S. K. Methods for Transferring Molecular Substances into Plant Cells. International Patent Publication 2009, WO2009/046384.

(16) Samuel, J. P.; Samboju, N. C.; Yau, K. Y.; Webb, S. R.; Burroughs, F. G. Use of Dendrimer Nanotechnology for Delivery of Biomolecules into Plant Cells. International Patent Publication 2011, WO2011/046786.

(17) Pepper, J. T.; Maheshwari, P.; Ziemienowicz, A.; Hazendonk, P.; Kovalchuk, I.; Eudes, F. Tetrabutylphosphonium Bromide Reduces Size and Polydispersity Index of Tat2:Sirna Nano-Complexes for Triticale RNAi. *Front. Mol. Biosci.* **2017**, *4*, 30.

(18) Liu, J.; Wang, F.; Wang, L.; Xiao, S.; Tong, C.; Tang, D.; Liu, X. Preparation of Fluorescence Starch-Nanoparticle and its Application as Plant Transgenic Vehicle. *J. Cent. South Univ. Technol.* **2008**, *15*, 768−773.

(19) Martin-Ortigosa, S.; Valenstein, J. S.; Lin, V. S. Y.; Trewyn, B. G.; Wang, K. Gold Functionalized Mesoporous Silica Nanoparticle Mediated Protein and DNA Co-Delivery to Plant Cells via the Biolistic Method. *Adv. Funct. Mater.* **2012**, *22*, 3576−3582.

(20) Cunningham, F. J.; Goh, N. S.; Demirer, G. S.; Matos, J. L.; Landry, M. P. Nanoparticle-Mediated Delivery towards Advancing Plant Genetic Engineering. *Trends Biotechnol.* **2018**, *36*, 882−897.

(21) Crossway, A.; Oakes, J. V.; Irvine, J. M.; Ward, B.; Knauf, V. C.; Shewmaker, C. K. Integration of Foreign DNA Following Micro-injection of Tobacco Mesophyll Protoplasts. *Mol. Gen. Genet.* **1986**, *202*, 179−185.

(22) Touraev, A.; Stoger, E.; Voronin, V.; Heberle-Bors, E. Plant male germ line transformation. *Plant J.* **1997**, *12*, 949−956.

(23) Ferrie, A. M. R. Doubled Haploid Production in Higher Plants. *Encycl. Appl. Plant Sci.* **2016**, *2*, 147−151.

(24) Pepper, J. T.; Maheshwari, P.; Eudes, F. Adsorption of Cell-Penetrating Peptide Tat2 and Polycation Luviquat FC-370 to Triticale Microspore Exine. *Colloids Surf., B* **2017**, *157*, 207−214.

(25) Andriy, B.; Justin, L.; Eudes, F. Intracellular Delivery of Fluorescent Protein into Viable Wheat Microspores Using Cationic Peptides. *Front. Plant Sci.* **2015**, *6*, 666.

(26) Kwak, S.-Y.; Lew, T. T. S.; Sweeney, C. J.; Koman, V. B.; Wong, M. H.; Bohmert-Tatarev, K.; Snell, K. D.; Seo, J. S.; Chua, N.-H.; Strano, M. S. Chloroplast-selective Gene Delivery and Expression in Planta using Chitosan-Somplexed Single-Walled Carbon Nanotube Carriers. *Nat. Nanotechnol.* **2019**, *14*, 447−455.

(27) Demirer, G. S.; Zhang, H.; Matos, J. L.; Goh, N. S.; Cunningham, F. J.; Sung, Y.; Chang, R.; Aditham, A. J.; Chio, L.; Cho, M.-J.; Staskawicz, B.; Landry, M. P. High Aspect Ratio Nanomaterials Enable Delivery of Functional Genetic Material without DNA Integration in Mature Plants. *Nat. Nanotechnol.* **2019**, *14*, 456−464.

(28) Hansen, S. F.; Lennquist, A. Carbon nanotubes added to the SIN List as a nanomaterial of Very High Concern. *Nat. Nanotechnol.* **2020**, *15*, 3−4.

(29) Fenniri, H.; Mathivanan, P.; Vidale, K. L.; Sherman, D. M.; Hallenga, K.; Wood, K. V.; Stowell, J. G. Helical Rosette Nanotubes: Design, Self-assembly and Characterization. *J. Am. Chem. Soc.* **2001**, *123*, 3854−3855.

(30) Beingessner, R. L.; Fan, Y.; Fenniri, H. Molecular and Supramolecular Chemistry of Rosette Nanotubes. *RSC Adv.* **2016**, *6*, 75820−75838.

(31) Moralez, J. G.; Raez, J.; Yamazaki, T.; Motkuri, R. K.; Kovalenko, A.; Fenniri, H. Helical Rosette Nanotubes with Tunable Stability and Hierarchy. *J. Am. Chem. Soc.* **2005**, *127*, 8307−8309.

(32) Johnson, R. S.; Yamazaki, T.; Kovalenko, A.; Fenniri, H. Molecular Basis For Water-Promoted Supramolecular Chirality Inversion In Helical Rosette Nanotubes. *J. Am. Chem. Soc.* **2007**, *129*, 5735−5743.

(33) Hemraz, U. D.; El-Bakkari, M.; Yamazaki, T.; Cho, J. Y.; Beingessner, R.; Fenniri, H. Chiromers: Conformation-driven Mirror-Image Supramolecular Chirality Isomerism Identified in a New Class of Helical Rosette Nanotubes. *Nanoscale* **2014**, *6*, 9421−9427.

(34) Journeay, W. S.; Suri, S. S.; Moralez, J. G.; Fenniri, H.; Singh, B. Rosette Nanotubes Show Low Acute Pulmonary Toxicity in Vivo. *Int. J. Nanomed.* **2008**, *3*, 373−383.

(35) Ede, J. D.; Ortega, V. A.; Boyle, D.; Beingessner, R. L.; Hemraz, U. D.; Fenniri, H.; Stafford, J.; Goss, G. Rosette Nanotubes Alter Ige-Mediated Degranulation in the Rat Basophilic Leukemia (RBL)-2H3 Cell Line. *Toxicol. Sci.* **2015**, *148*, 108−120.

(36) Ede, J. D.; Ortega, V. A.; Boyle, D.; Beingessner, R. L.; Hemraz, U. D.; Fenniri, H.; Stafford, J. L.; Goss, G. The Effects of Rosette Nanotubes with Different Functionalizations on Channel Catfish (*Ictalurus punctatus*) Lymphocyte Viability and Receptor Function. *Environ. Sci.: Nano* **2016**, *3*, 578−592.

(37) Chun, A. L.; Moralez, J. G.; Webster, T. J.; Fenniri, H. Helical Rosette Nanotubes: a Biomimetic Coating for Orthopedics? *Biomaterials* **2005**, *26*, 7304−7309.

(38) Fine, E.; Zhang, L.; Fenniri, H.; Webster, T. J. Enhanced endothelial cell functions on rosette nanotube-coated titanium vascular stents. *Int. J. Nanomed.* **2009**, *4*, 91−97.

(39) Zhang, L.; Rakotondradany, F.; Myles, A. J.; Fenniri, H.; Webster, T. J. Arginine-Glycine-Aspartic Acid Modified Rosette Nanotube-Hydrogel Composites for Bone Tissue Engineering. *Biomaterials* **2009**, *30*, 1309−1320.

(40) Zhang, L.; Hemraz, U. D.; Fenniri, H.; Webster, T. J. Tuning Cell Adhesion on Titanium with Osteogenic Rosette Nanotubes. *J. Biomed. Mater. Res., Part A* **2010**, *95*, 550−563.

(41) Chen, Y.; Bilgen, B.; Pareta, R. A.; Myles, A. J.; Fenniri, H.; Ciombor, D. M.; Aaron, R. K.; Webster, T. J. Self-assembled Rosette Nanotube/Hydrogel Composites for Cartilage Tissue Engineering. *Tissue Eng., Part C* **2010**, *16*, 1233−1243.

(42) Sun, L.; Zhang, L.; Hemraz, U. D.; Fenniri, H.; Webster, T. Bioactive Rosette Nanotube Hydroxy-Apatite Nanocomposites Improve Osteoblast Functions. *Tissue Eng., Part A* **2012**, *18*, 1741−1750.

(43) Meng, X.; Stout, D. A.; Sun, L.; Beingessner, R. L.; Fenniri, H.; Webster, T. J. Novel Injectable Biomimetic Hydrogels with Carbon Nanofibers and Self-Assembled Rosette Nanotubes for Myocardial Applications. *J. Biomed. Mater. Res., Part A* **2013**, *101*, 1095−1102.

(44) Childs, A.; Hemraz, U. D.; Castro, N. J.; Fenniri, H.; Zhang, L. G. Novel Biologically-Inspired Rosette Nanotube PLLA Scaffolds for Improving Human Mesenchymal Stem Cell Chondrogenic Differentiation. *Biomed. Mater.* **2013**, *8*, No. 065003.

(45) Sun, L.; Li, D.; Hemraz, U. D.; Fenniri, H.; Webster, T. J. Self-assembled Twin Base Linker and Poly(2-Hydroxyethyl Methacrylate) Hydrogels Promote Skin Cell Functions. *J. Biomed. Mater. Res., Part A* **2014**, *102*, 3446−3451.

(46) Puzan, M. L.; Legesse, B.; Koppes, R. A.; Fenniri, H.; Koppes, A. N. Bioactive Organic Rosette Nanotubes Support Sensory Neurite Outgrowth. *ACS Biomater. Sci. Eng.* **2018**, *4*, 1630−1640.

(47) Bhowmik, P.; Ellison, E.; Polley, B.; Bollina, V.; Kulkarni, M.; Ghanbarnia, K.; Song, H.; Gao, C.; Voytas, D. F.; Kagale, S. Targeted Mutagenesis in Wheat Microspores using CRISPR/Cas9. *Sci. Rep.* **2018**, *8*, No. 6502.

(48) Eudes, F.; Amundsen, E. Isolated microspore culture of Canadian 6 × triticale cultivars. *Plant Cell, Tissue Organ Cult.* **2005**, *82*, 233−241.

(49) Morimoto, K.; Nishikawa, M.; Kawakami, S.; Nakano, T.; Hattori, Y.; Fumoto, S.; Yamashita, F.; Hashida, M. Molecular Weight-Dependent Gene Transfection Activity of Unmodified and Galactosylated Polyethyleneimine on Hepatoma Cells and Mouse Liver. *Mol. Ther.* **2003**, *7*, 254−261.

(50) Kunath, K.; von Harpe, A.; Fischer, D.; Petersen, H.; Bickel, U.; Voigt, K.; Kissel, T. Low molecular weight polyethylenimine as a non-viral vector for DNA delivery: Comparison of Physicochemical Properties, Transfection Efficiency and In Vivo Distribution with High Molecular Weight Polyethylenimine. *J. Controlled Release* **2003**, *89*, 113−125.

(51) Ogris, M.; Steinlein, P.; Kursa, M.; Mechtler, K.; Kircheis, R.; Wagner, E. The Size of DNA/Transferrin-PEI Complexes is an Important Factor for Gene Expression In Cultured Cells. *Gene Ther.* **1998**, *5*, 1425−1433.

(52) Weecharangsan, W.; Opanasopit, P.; Ngawhirunpat, T.; Apirakaramwong, A.; Rojanarata, T.; Ruktanonchai, U.; Lee, R. J. Evaluation of Chitosan Salts as Non-Viral Gene Vectors in Cho-K1 Cells. *Int. J. Pharm.* **2008**, *348*, 161−168.

(53) Zheng, M. Y.; Liu, W.; Weng, Y.; Polle, E.; Konzak, C. F. Culture of Freshly Isolated Wheat (*Triticum Aestivum* L.) Microspores Treated with Inducer Chemicals. *Plant Cell Rep.* **2001**, *20*, 685−690.

(54) Suri, S. S.; Mills, S.; Aulakh, G. K.; Rakotondradany, F.; Fenniri, H.; Singh, B. RGD-tagged Helical Rosette Nanotubes Aggravate Acute Lipopolysaccharide-Induced Lung Inflammation. *Int. J. Nanomed.* **2011**, *6*, 3113−3123.

(55) Modra, K.; Dai, S.; Zhang, H.; Shi, B.; Bi, J. Polycation-Mediated Gene Delivery: Challenges and Considerations for the Process of Plasmid DNA Transfection. *Eng. Life Sci.* **2015**, *15*, No. 489498.

(56) Luten, J.; vanNostruin, C. F.; DeSmedt, S. C.; Hennink, W. E. Biodegradable Polymers as Non-Viral Carriers for Plasmid DNA Delivery. *J. Controlled Release* **2008**, *126*, 97−110.

(57) Ghafari, P.; St-Denis, C. H.; Power, M. E.; Jin, X.; Tsou, V.; Mandal, H. S.; Bols, N. C.; Tang, X. S. Impact of Carbon Nanotubes on the Ingestion and Digestion of Bacteria by Ciliated Protozoa. *Nat. Nanotechnol.* **2008**, *3*, 347−351.

(58) Tejral, G.; Panyala, N. R.; Havel, J. Carbon Nanotubes: Toxicological Impact on Human Health and Environment. *J. Appl. Biomed.* **2009**, *7*, 1−13.